

Enhancement of Piezoelectricity in a Mixed Ferroelectric

Eric Cockayne and Karin M. Rabe

Department of Applied Physics, Yale University, P.O. Box 208284, New Haven, CT 06520-8284
(January 10, 2022)

We use first-principles density-functional total energy and polarization calculations to calculate the piezoelectric tensor at zero temperature for both cubic and simple tetragonal ordered supercells of Pb_3GeTe_4 . The largest piezoelectric coefficient for the tetragonal configuration is enhanced by a factor of about three with respect to that of the cubic configuration. This can be attributed to both the larger strain-induced motion of cations relative to anions and higher Born effective charges in the tetragonal case. A normal mode decomposition shows that both cation ordering and local relaxation weaken the ferroelectric instability, enhancing piezoelectricity.

Piezoelectric materials are of great technological importance. The highest known piezoelectric coefficients are found in mixed compounds, such as $\text{Pb}(\text{Zr}_{1-x}\text{Ti}_x)\text{O}_3$ near its morphotropic phase boundary at $x \approx 0.45$. This association has been reinforced by the recent discovery of giant piezoelectricity in single crystals of the relaxor ferroelectric systems $\text{Pb}(\text{A}_{1/3}\text{Nb}_{2/3})\text{O}_3\text{-PbTiO}_3$, ($\text{A} = \text{Zn}, \text{Mg}$). [1] Understanding of the physical origin of enhancement of piezoelectricity in mixed ferroelectrics would be of great theoretical interest and could also point to new ways to tune this property.

Ab initio calculations have proved successful in relating properties of ferroelectrics to phenomena on the atomic level. Structural parameters [2,3], dielectric constants, effective charges and phonon dispersion relations [4,5], and structural phase transition temperatures [6] have been calculated from first principles. Such methods can naturally be extended to piezoelectricity. Piezoelectric coefficients have been calculated from first principles for various materials [7–9], where good agreement with experimental results is obtained. For mixed systems, *ab initio* calculations can be performed on individual ordered supercells and the results analyzed to understand the dependence on configuration and the resulting ensemble average. In this Letter, we consider the mixed ferroelectric $\text{Pb}_{0.75}\text{Ge}_{0.25}\text{Te}$. Calculation of the piezoelectric response shows significant configuration dependence, with enhancement of piezoelectricity in the cell with lower symmetry. We interpret and explain the results in terms of chemical bonding and long range dipolar interactions.

$\text{Pb}_{1-x}\text{Ge}_x\text{Te}$ undergoes a transition from a paraelectric cubic rocksalt phase at high temperature to a ferro-

electric rhombohedral phase at low temperature, dominated by Ge off-centering [10], for all compositions $x > 0.005$. [11]. In order to study the dilute Ge limit while maintaining small supercells, we choose $x = 0.25$. The configurations which we investigate are shown in Figure 1. The structures have identical compositions Pb_3GeTe_4 , but one is simple cubic (cP8) and one is simple tetragonal (tP8).

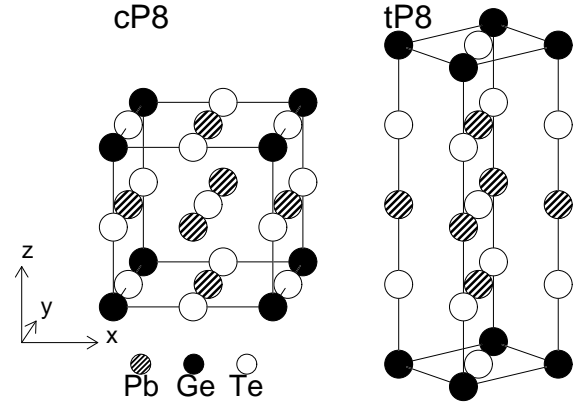


FIG. 1. Pb_3GeTe_4 cP8 and tP8 configurations.

First-principles density-functional calculations were performed using the program CASTEP 2.1 [12], with a plane wave basis set in the local density approximation. Bachelet-Hamann-Schlüter pseudopotentials [13] were used for all atoms. For the cP8 configuration, we used a $4 \times 4 \times 4$ Monkhorst-Pack set of \mathbf{k} points; for the tP8 configuration, we used the same \mathbf{k} point grid, folded into the tetragonal Brillouin zone. In our study of the structural phase transition in the Pb_3GeTe_4 -cP8 configuration [14], we give further details on the *ab initio* calculations. Fixing the atoms in rocksalt positions and minimizing total energies with respect to strain, we obtained $a = 6.275 \text{ \AA}$ for cP8 and $a = 4.438 \text{ \AA}$; $c = 12.548 \text{ \AA}$ for tP8. These are taken as the high symmetry reference structures for the two configurations. Next, we determined the ground state structures. For a series of fixed global strains, as many as 6 independent internal coordinates in the cP8 configuration and 16 internal coordinates in the tP8 configuration were relaxed via conjugate gradients minimization. In each relaxation, we broke the initial symmetry by displacing each Ge atom by 0.3 \AA in the (111) direction. A quadratic fit of total energies as a function of strain was used to find the equilibrium strain. The cP8 ground state obtained is rhombohedral, space group

R3m, $a = 6.315 \text{ \AA}$, $\alpha = 89.47^\circ$, and the tP8 ground state is monoclinic, space group Pm, $a = 4.497 \text{ \AA}$, $b = 4.409 \text{ \AA}$, $c = 12.575 \text{ \AA}$, $\beta = 89.31^\circ$. The internal coordinates are given in Table I, with the center of mass fixed in each case to that of a strained rocksalt structure with Ge on the origin.

The method of King-Smith and Vanderbilt (KSV) [15] was then used to calculate polarizations. This method calculates the *electronic* contribution to the polarization, to which the ionic contribution is added to obtain the total polarization \mathbf{P} . The component of polarization along lattice vector \mathbf{a}_α is expressed in terms of a set of wavefunction calculations along straight-line paths in the Brillouin zone, where reciprocal lattice vector \mathbf{b}_α is the path vector, J the number of \mathbf{k} points in the path, and \mathbf{k}_\perp the component of \mathbf{k} orthogonal to \mathbf{b}_α along the path.

In Voigt notation, the components of the (third rank) piezoelectric strain tensor are given by $e_{\alpha\beta} \equiv \partial P_\alpha / \partial \epsilon_\beta$, where ϵ_α is a component of the (second rank) strain tensor. We used finite differences to determine the piezoelectric tensor components: $e_{\alpha\beta} \approx \Delta P_\alpha / \Delta \epsilon_\beta$. For both the cP8 and tP8 configurations, we calculated \mathbf{P} for the ground states and for a set of fully relaxed strained cells with one strain component ϵ_α increased by 0.005. Strains were measured with respect to the axes shown in Figure 1. Strain magnitudes were measured with respect to the cP8 reference structure ($a = 6.275 \text{ \AA}$) in both cases. The KSV calculations were performed using the self-consistent potentials obtained from total energy calculations using 64 \mathbf{k} points in the Brillouin Zone. We used $J = 32$ for cP8, $J = 16$ for tP8 along \mathbf{b}_3 , and $J = 48$ for tP8 along \mathbf{b}_1 and \mathbf{b}_2 . In each case, we obtained the cross section average by averaging the values for \mathbf{k}_\perp on a 4×4 Monkhorst-Pack grid. These parameters were sufficient to converge the piezoelectric tensor components to within $0.05 C/m^2$.

The resultant piezoelectric tensor components and their decomposition into clamped ion and internal strain contributions [8] are shown in Table II. Generally, the components in the tP8 configuration are larger in magnitude than in the cP8 one. The clamped ion terms are remarkably similar; the differences are almost entirely due to internal strain. We will focus on e_{33} because it is the largest piezoelectric component in each case and shows the greatest change in going from the cP8 to the tP8 configuration.

We first look at the configuration dependence of the internal strain term $e_{33}|_{\text{int}}$ by analyzing the contributions of individual ions:

$$e_{33}|_{\text{int}} = \frac{1}{V} \sum_{i\alpha} \mathbf{Z}_{i,z\alpha}^* \frac{\partial u_{i\alpha}}{\partial \epsilon_3}, \quad (1)$$

where \mathbf{Z}_i^* are the Born effective charge tensors and $\partial \mathbf{u}_i / \partial \epsilon_3$ is the movement of the relaxed ion position from the clamped ion position with strain (in fixed center of

mass coordinates). For each configuration, we determined \mathbf{Z}_i^* from the changes in polarization resulting from displacing each atom in turn 0.01 \AA along each axis direction, and $\partial \mathbf{u}_i / \partial \epsilon_3$ by comparing the relaxed coordinates of the ions in the two cells differing only in ϵ_3 . Since the displacement derivatives $\partial \mathbf{u}_i / \partial \epsilon_3$ are dominated by motion in the \hat{z} direction, we make the following approximation:

$$e_{33}|_{\text{int}} \approx \tilde{e}_{33}|_{\text{int}} \equiv \frac{1}{V} \sum_i \mathbf{Z}_{i,zz}^* \frac{\partial u_{iz}}{\partial \epsilon_3} \equiv \sum_i^{\text{unit cell}} \tilde{e}_{33}^{(i)}|_{\text{int}} \quad (2)$$

The calculated values for $\partial u_{iz} / \partial \epsilon_3$ and $\mathbf{Z}_{i,zz}^*$ are given for each ion in Table III.

For both the cP8 and tP8 configurations, the values of $\tilde{e}_{33}|_{\text{int}}$ obtained from Eq. 2 agree with $e_{33}|_{\text{int}}$ to better than 6%. The values of Table III can thus be used to associate the enhancement of piezoelectricity in tP8 with the response of the individual ions. It can be seen that the increased ionic motion under strain is the dominant factor, with additional enhancement due to the larger average magnitude of the Born effective charges. Both the magnitude of the piezoelectric response and the configuration dependence is greatest in the chains along \hat{z} containing the Ge ions.

The theory of resonant p-bonding [16,17] in IV-VI compounds gives insight into this trend. In the symmetric rocksalt structure, the covalent bonds are composed primarily of p orbitals, with one electron per bond. In each anion-cation-anion segment, there is thus the tendency for the cation to prefer an off-center position, forming a short cation-anion bond on one side into which the electron from the long bond is partially transferred. The off-centering is therefore associated with a large \mathbf{Z}^* . This tendency is counterbalanced by short range repulsion, the strength of which is roughly determined by the ionic radius of the cation. In pure PbTe, short-range repulsion dominates and the low temperature structure is rocksalt [17], while in GeTe, the off-centering instability dominates and the low temperature structure is rhombohedral. In $\text{Pb}_{0.985}\text{Ge}_{0.015}$, the low temperature structure is rhombohedral at low pressure and cubic at high pressure [18], showing that the relative importance of the short-range repulsion increases with pressure.

Equivalently, a decrease in the Te-cation-Te distance suppresses off-centering. Figure 2 shows the z -component of the polarization of pure GeTe and PbTe as a function of lattice parameter, fit to the results of KSV calculations in which internal relaxation is allowed but the lattice is held cubic. A ferroelectric instability is predicted for PbTe at sufficient negative pressure. In the mixed system, we define *local* lattice parameters along \hat{z} to be equal to the Te-cation-Te distance, and qualitatively associate the local piezoelectric response with the slope of the P_z vs. a curve for the corresponding pure cation-Te system. In the cP8 configuration, there is a single local

lattice parameter, the value of which favors off-centering and piezoelectric response for the Te-Ge-Te chain but not for the Te-Pb-Te chains. In the tP8 configuration, there is a different type of chain, with alternating Ge and Pb. In this chain, relaxation of the Te ions along \hat{z} leads to two effective local lattice constants: a short Te-Ge-Te and a large Te-Pb-Te distance marked in Figure 2. The latter Te-Pb-Te distance is considerably larger than in pure PbTe, favoring off-centering and piezoelectric response in the Te-Pb-Te segment as well as the Te-Ge-Te segment, as seen in Table III.

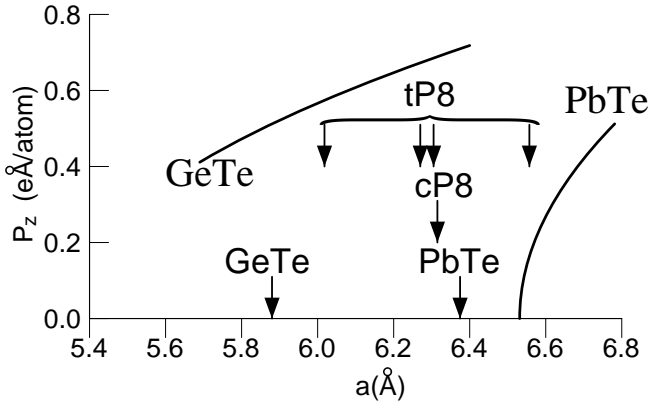


FIG. 2. Polarization vs. lattice parameter in PbTe and GeTe and first-principles LDA “local lattice parameters” along \hat{z} for PbTe, GeTe and mixed Pb_3GeTe_4 configurations

Another informative way to analyze the piezoelectric response is to decompose the ionic displacements into the contributions of the zone-center normal modes of the system. For the decomposition of $\tilde{e}_{33|int}$, we need only the polar modes of the high symmetry reference structures involving ionic motion along \hat{z} . For the tP8 systems, two reference structures were considered. One, tP8_{un} , has all ions sitting on ideal rocksalt coordinates, the other, tP8_{rel} , is derived from tP8_{un} via a *symmetry preserving* relaxation. In this relaxation, the Te atoms in the $z = \pm 0.25$ plane move $\mp 0.143\hat{z}$ Å and the Pb atoms in the $z = \pm 0.25$ plane move $\mp 0.029\hat{z}$ Å. The \hat{z} polar modes were determined from first principles frozen phonon calculations, as in Ref. [14], with the results given in Table IV. For each reference structure, one mode has imaginary frequency, indicating instability to a symmetry-breaking distortion.

The approximate piezoelectric response $\tilde{e}_{33|int}$ for a given ground state can be decomposed into normal mode contributions:

$$\tilde{e}_{33|int} = \frac{1}{V} \sum_{\mu} \bar{Z}_{\mu}^* \frac{\partial \xi_{\mu}}{\partial \epsilon_3}, \quad (3)$$

where mode effective charges are given by $\bar{Z}^* = \sum_i^{\text{unit cell}} Z_{i,z}^* (\partial u_{iz} / \partial \xi_{\mu})$ and $\partial \xi_{\mu} / \partial \epsilon_3$ is the change in the amplitude of mode μ with strain. All modes are normalized so that the sum of the squared atomic displacements is 1 Å² per 8-atom cell.

The results are shown in Table IV. In each case, the largest mode contribution is from the unstable mode. In fact, the unstable tP8_{rel} mode accounts for 97% of $\tilde{e}_{33|int}$ for tP8. We find that the relative Pb(3) motion in the unstable mode goes from 0.16 for tP8_{un} to 0.49 for tP8_{rel} , in agreement with the local viewpoint that a sufficient increase in the Te-Pb-Te distance will favor Pb off-centering and piezoelectric response.

We investigated the unstable mode contribution in greater depth by constructing a simple “double well” parametrization of the energy as a function of the amplitude of unstable mode distortion and strain ϵ_3 . When all other parameters are equal, decreasing the strength of the quadratic instability increases the piezoelectric response associated with the unstable mode. This trend is clear in Table IV. The weakening of the tP8_{un} instability relative to the cP8 instability is the result of the change in cationic configuration and is due largely to less favorable dipole-dipole interactions. Symmetry-preserving relaxation further weakens the instability and leads to an even greater unstable mode response.

As $\nu^2 \rightarrow 0^-$ for an unstable mode, the associated piezoelectric response will *diverge*. In stoichiometric ferroelectrics, this is essentially what happens at the paraelectric-ferroelectric transition, with a corresponding divergence in the piezoelectric coefficients on the low-symmetry side. In substitutionally disordered compounds containing one stable and one unstable endmember, such as $\text{Pb}_{1-x}\text{Ge}_x\text{Te}$, there will be a variety of local environments and therefore a range in the degree of local (in)stabilities. We expect in such systems that enhanced piezoelectricity can be observed for a range of temperatures, pressures and applied fields where the density of marginally unstable optical modes is significant. Even at fixed composition, the type of ordering present has a dramatic effect on the local stability and could be used to tune the piezoelectricity, (*e.g.* through control of processing or in epitaxial thin films). Quantitative modeling of the temperature-dependent response associated with the unstable modes of particular configuration, using the effective Hamiltonian approach [19], is currently in progress.

In conclusion, we have compared the piezoelectricity in two Pb_3GeTe_4 configurations and found strong enhancement of e_{33} in the tetragonal configuration. This effect is intrinsic; it will occur even in a single grain, single phase sample. The interpretation of the calculated results in terms of local polar instabilities and the long-range interactions between them suggests further opportunities for identification of solid solutions with large piezoelectric response.

This work was supported by ONR N00014-97-J-0047. We thank Volker Heine for stimulating discussions.

- [1] S.-E. Park and T. R. Strout, in *1996 IEEE Ultrasonics Symposium Proceedings* (New York: IEEE, 1996), v.2, p. 935; *J. Appl. Phys.* **82**, 1804 (1997), and references therein.
- [2] R. E. Cohen, *Nature* **358**, 136 (1992).
- [3] D. J. Singh, *Phys. Rev. B* **52**, 12559 (1995).
- [4] S. Baroni, P. Giannozzi and A. Testa, *Phys. Rev. Lett.* **58**, 1861 (1987).
- [5] X. Gonze, D. C. Allan and M. P. Teter, *Phys. Rev. Lett.* **68**, 3603 (1992).
- [6] K. M. Rabe and J. D. Joannopoulos, *Phys. Rev. Lett.* **59**, 570 (1987).
- [7] S. de Gironcoli, S. Baroni and R. Resta, *Phys. Rev. Lett.* **62**, 2853 (1989).
- [8] A. Dal Corso, M. Posternak, R. Resta and A. Baldereschi, *Phys. Rev. B* **50**, 10715 (1994).
- [9] G. Saghi-Szabo, R. E. Cohen and H. Krakauer, unpublished.
- [10] Yu. A. Logachev and B. Ya. Moizhes, *Sov. Phys. Solid State* **19**, 1635 (1977). (*Fiz. Tverd. Tela* (Leningrad) **19**, 2793 (1977)).
- [11] S. Takaoka and K. Murase, *Phys. Rev. B* **20**, 2823 (1979).
- [12] M. C. Payne, X. Weng, B. Hammer, G. Francis, I. Stich, U. Bertram, A. de Vita, J. S. Lin. A. Qteish and V. Milman, “CASTEP 2.1”, Cavendish Laboratory, University of Cambridge (1991).
- [13] G. B. Bachelet, D. R. Hamann and M. Schlüter, *Phys. Rev. B* **26**, 4199 (1982).
- [14] E. Cockayne and K. M. Rabe, *Phys. Rev. B* **56**, 7947 (1997).
- [15] R. D. King-Smith and D. Vanderbilt, *Phys. Rev. B* **47**, 1651 (1993).
- [16] G. Lucovsky and R. M. White, *Phys. Rev. B* **8**, 660 (1973).
- [17] P. B. Littlewood, *CRC Crit. Rev. in Solid State and Mat. Sci.* **11**, 229 (1984).
- [18] T. Suski, S. Takaoka and K. Murase, *Solid State Communications* **45**, 259 (1983).
- [19] K. M. Rabe and U. V. Waghmare, *Phys. Rev. B* **52**, 13236 (1995).

TABLE I. *Ab initio* ground state structures of Pb_3GeTe_4 cP8 and tP8 configurations. Lattice constants given in text.

cP8				tP8			
Atom	x	y	z	Atom	x	y	z
Pb(1)	0.0014	0.5037	0.5037	Pb(1)	0.5120	0.5	0.2485
Pb(2)	0.5037	0.0014	0.5037	Pb(2)	0.4961	0.5	0.7516
Pb(3)	0.5037	0.5037	0.0014	Pb(3)	0.0054	0	0.5065
Ge	0.0308	0.0308	0.0308	Ge	0.0576	0	0.0062
Te(1)	0.9985	0.9985	0.4760	Te(1)	0.9985	0	0.2349
Te(2)	0.9985	0.4760	0.9985	Te(2)	0.9849	0	0.7563
Te(3)	0.4760	0.9985	0.9985	Te(3)	0.4661	0.5	0.9980
Te(4)	0.4955	0.4955	0.4955	Te(4)	0.4958	0.5	0.4966

TABLE II. Comparison of piezoelectric tensors for the ground states of two Pb_3GeTe_4 configurations (in C/m^2). Components in parentheses are equal to other components via symmetry.

Component	Total		Clamped ion		Internal strain	
	cP8	tP8	cP8	tP8	cP8	tP8
e_{11}	1.8	2.5	-0.5	-0.5	2.3	3.0
e_{12}	-0.6	-1.2	0.0	0.0	-0.6	-1.2
e_{13}	(-0.6)	-0.9	(0.0)	0.0	(-0.6)	-0.9
e_{14}	-0.2	-0.6	0.0	0.0	-0.2	-0.6
e_{15}	1.0	1.2	0.6	0.5	0.4	0.7
e_{16}	(1.0)	1.1	(0.6)	0.5	(0.4)	0.6
e_{31}	(-0.6)	-0.3	(0.0)	0.0	(-0.6)	-0.3
e_{33}	(1.8)	5.1	(-0.5)	-0.5	2.3	5.6
e_{34}	(1.0)	2.2	(0.6)	0.7	(0.4)	1.5
e_{36}	(-0.2)	-0.5	(0.0)	0.0	(-0.2)	-0.5

TABLE III. Contributions of individual ions to e_{33}^{int} in Pb_3GeTe_4 cP8 and tP8 configurations. Atoms located in chains along \hat{z} containing Ge are italicized. $\tilde{e}_{33}^{(i)}|_{\text{int}}$ are in C/m^2 ; $\frac{\partial u_{iz}}{\partial \epsilon_3}$ in Å.

cP8				tP8			
Atom	$Z_{i,zz}^*$	$\frac{\partial u_{iz}}{\partial \epsilon_3}$	$\tilde{e}_{33}^{(i)} _{\text{int}}$	Atom	$Z_{i,zz}^*$	$\frac{\partial u_{iz}}{\partial \epsilon_3}$	$\tilde{e}_{33}^{(i)} _{\text{int}}$
Pb(1)	5.4	0.72	0.25	Pb(1)	5.9	0.32	0.12
Pb(2)	5.4	0.72	0.25	Pb(2)	5.8	0.91	0.34
Pb(3)	5.9	0.91	0.34	<i>Pb(3)</i>	5.6	3.08	1.11
Ge	3.1	0.79	0.16	<i>Ge</i>	5.7	2.60	0.95
<i>Te(1)</i>	-4.0	-3.08	0.78	<i>Te(1)</i>	-5.9	-3.11	1.18
Te(2)	-5.0	-0.37	0.12	<i>Te(2)</i>	-5.7	-2.80	1.03
Te(3)	-5.0	-0.37	0.12	Te(3)	-5.5	-0.83	0.29
Te(4)	-5.8	-0.46	0.17	Te(4)	-5.9	-1.74	0.66

TABLE IV. Polar mode contribution to $\tilde{e}_{33}|_{int}$ in Pb_3GeTe_4 -cP8 and tP8. cP8 and tP8 modes have symmetry labels Γ_{15}^z and Γ_1' , respectively. \bar{Z}_μ^* are in eÅ; $\tilde{e}_{33}|_{int}^{(\mu)}$ in C/m^2 and ν_μ in cm^{-1} .

cP8				tP8 _{un}				tP8 _{rel}			
ν_μ	\bar{Z}_μ^*	$\partial\xi_\mu/\partial\epsilon_3$	$\tilde{e}_{33} _{int}^{(\mu)}$	ν_μ	\bar{Z}_μ^*	$\partial\xi_\mu/\partial\epsilon_3$	$\tilde{e}_{33} _{int}^{(\mu)}$	ν_μ	\bar{Z}_μ^*	$\partial\xi_\mu/\partial\epsilon_3$	$\tilde{e}_{33} _{int}^{(\mu)}$
103 i	5.9	2.93	1.09	64 i	11.5	6.28	4.64	40 i	13.6	6.32	5.53
31	1.6	1.09	0.11	42	2.9	-0.14	-0.03	42	5.2	0.64	0.22
46	4.2	2.44	0.65	85	6.6	3.30	1.41	89	3.1	-0.62	-0.12
82	10.6	0.52	0.34	102	3.6	-1.08	-0.25	95	4.2	0.46	0.12
105	1.0	-0.23	-0.01	117	1.3	-1.20	-0.10	122	4.0	-0.28	-0.07